HHS Public Access

Author manuscript

J Vis Exp. Author manuscript; available in PMC 2020 July 01.

Visualizing Protein Kinase A Activity In Head-fixed Behaving Mice Using In Vivo Two-photon Fluorescence Lifetime Imaging Microscopy

Bart C. Jongbloets[*,1], **Lei Ma**[*,1], **Tianyi Mao**[1], **Haining Zhong**[1]

[1]Vollum Institute, Oregon Health & Science University

Abstract

Neuromodulation exerts powerful control over brain function. Dysfunction of neuromodulatory systems results in neurological and psychiatric disorders. Despite their importance, technologies for tracking neuromodulatory events with cellular resolution are just beginning to emerge. Neuromodulators, such as dopamine, norepinephrine, acetylcholine, and serotonin, trigger intracellular signaling events via their respective G protein-coupled receptors to modulate neuronal excitability, synaptic communications, and other neuronal functions, thereby regulating information processing in the neuronal network. The above mentioned neuromodulators converge onto the cAMP/protein kinase A (PKA) pathway. Therefore, in vivo PKA imaging with single-cell resolution was developed as a readout for neuromodulatory events in a manner analogous to calcium imaging for neuronal electrical activities. Herein, a method is presented to visualize PKA activity at the level of individual neurons in the cortex of head-fixed behaving mice. To do so, an improved A-kinase activity reporter (AKAR), called tAKARα, is used, which is based on Förster resonance energy transfer (FRET). This genetically-encoded PKA sensor is introduced into the motor cortex via in utero electroporation (IUE) of DNA plasmids, or stereotaxic injection of adeno-associated virus (AAV). FRET changes are imaged using two-photon fluorescence lifetime imaging microscopy (2pFLIM), which offers advantages over ratiometric FRET measurements for quantifying FRET signal in light-scattering brain tissue. To study PKA activities during enforced locomotion, tAKARα is imaged through a chronic cranial window above the cortex of awake, head-fixed mice, which run or rest on a speed-controlled motorized treadmill. This imaging approach will be applicable to many other brain regions to study corresponding behavior-induced PKA activities and to other FLIM-based sensors for in vivo imaging.

Keywords

Neuroscience; Issue 148; neuromodulation; cAMP-dependent protein kinase/protein kinase A (PKA); A-kinase activity reporter (AKAR); Förster resonance energy transfer (FRET); tAKARα; in vivo two-photon fluorescence lifetime imaging microscopy (2pFLIM); craniotomy; locomotion

Correspondence to: Bart C. Jongbloets at jongbloe@ohsu.edu, Haining Zhong at zhong@ohsu.edu.
*These authors contributed equally

Disclosures
The authors have nothing to disclose.

Video Link
The video component of this article can be found at https://www.jove.com/video/59526/

Introduction

Neuromodulation, also known as slow synaptic transmission, imposes strong control over brain function during different behavioral states, such as stress, arousal, attention, and locomotion[1,2,3,4]. Despite its importance, the study of when and where neuromodulatory events take place is still in its infancy. Neuromodulators, including acetylcholine, dopamine, noradrenaline, serotonin, and many neuropeptides, activate G protein-coupled receptors (GPCRs), which in turn trigger intracellular second messenger pathways with a wide window of timescales ranging from seconds to hours. While each neuromodulator triggers a distinct set of signaling events, the cAMP/protein kinase A (PKA) pathway is a common downstream pathway for many neuromodulators[1,5]. The cAMP/PKA pathway regulates neuronal excitability, synaptic transmission, and plasticity[6,7,8,9], and therefore, tunes the neuronal network dynamics. Because different neurons or neuronal types express different types or levels of neuromodulator receptors[10], the intracellular effects of the same extracellular neuromodulator may be heterogeneous across different neurons, and thus, have to be studied with cellular resolution. To date, it remains challenging to monitor neuromodulatory events in individual neurons in vivo during behavior.

To study the spatiotemporal dynamics of neuromodulation, a suitable recording modality is required. Microdialysis and fast-scan cyclic voltammetry are frequently used to study release of neuromodulators, but they lack the spatial resolution to monitor cellular events[11,12]. Analogous to calcium dynamics being used as a proxy for neuronal electrical activity in population imaging[13], PKA imaging may be used to read out neuromodulatory events across a neuronal population at cellular resolution. The present protocol describes the use of an improved A-kinase activity reporter (AKAR) to monitor PKA activities in vivo during animal behavior. The method described here allows for simultaneous imaging of neuronal populations at subcellular resolution with a temporal resolution that tracks physiological neuromodulatory events.

AKARs are composed of a donor and an acceptor fluorescent proteins linked by a PKA phosphorylation substrate peptide and a forkheadassociated (FHA) domain that binds to the phosphorylated serine or threonine of the substrate[14,15]. Upon activation of the PKA pathway, the substrate peptide of AKAR is phosphorylated. As a result, the FHA domain binds to the phosphorylated substrate peptide, thereby bringing the two fluorophores into close proximity, referred to as the closed state of AKAR. The closed state of a phosphorylated AKAR results in increased Förster resonance energy transfer (FRET) between the donor and acceptor fluorophores. Since the proportion of phosphorylated AKARs is related to the level of PKA activity[16], the amount of FRET in a biological sample can be used to quantify the level of PKA activity[16,17,18,19,20].

Early versions of AKARs were primarily designed for two-color ratiometric imaging[14]. When imaging deeper into brain tissue, the ratiometric method suffers from signal distortion due to wavelength-dependent light scattering[17,18,21]. As discussed below, fluorescence lifetime imaging microscopy (FLIM) eliminates this problem because FLIM only measures photons emitted by the donor fluorophore[18,21]. As a result, FLIM quantification of FRET is

not affected by the tissue-depth[17]. In addition, a “dark” (i.e., low quantum yield [QY]) variant of the acceptor fluorophore can be used. This frees a color channel to facilitate multiplexed measurement of orthogonal neuronal properties via simultaneous imaging of a second sensor or a morphological marker[17,19,20].

FLIM imaging quantifies the time that a fluorophore spends in the excited state, i.e., the fluorescence lifetime[18]. The return of a fluorophore to the ground state, thus the end of the excited state, often concomitates with the emission of a photon. Although the emission of a photon for an individual excited molecule is stochastic, in a population the mean fluorescence lifetime is a characteristic of that particular fluorophore. When a pure population of fluorophores are excited simultaneously, the resulting fluorescence will follow a single exponential decay. The time constant of this exponential decay corresponds to the mean fluorescence lifetime, which typically ranges from one to four nanoseconds for fluorescent proteins. The return of an excited donor fluorophore to the ground state can also occur by FRET. In the presence of FRET, the fluorescence lifetime of the donor fluorophore is reduced. The unphosphorylated AKARs exhibit a relatively longer donor fluorescence lifetime. Upon phosphorylation by PKA, the sensor exhibits a shorter lifetime because the donor and acceptor fluorophores are brought near each other and FRET is increased. The quantification of the fluorescence lifetime in a population of AKARs therefore represents the level of PKA activity.

Early versions of AKARs have not been successfully used for in vivo imaging at single-cell resolution. This is mainly due to the low signal amplitude of the AKAR sensors to physiological activations[17]. Recently, by systematically comparing available AKAR sensors for two-photon fluorescence lifetime imaging microscopy (2pFLIM), a sensor called FLIM-AKAR was found to outperform alternative sensors. Furthermore, a series of FLIM-AKAR variants called targeted AKARs (tAKARs) were developed to visualize PKA activity at specific subcellular locations: microtubules (tAKARα), cytosol (tAKARβ), actin (tAKARδ), filamentous actin (tAKARε), membrane (tAKARγ), and postsynaptic density (tAKARζ). Among tAKARs, tAKARα increased the signal amplitude elicited by norepinephrine by 2.7-fold. This is consistent with the knowledge that the majority of PKA in neurons are anchored to microtubules at the resting state[22,23]. tAKARα was the best performer among existing AKARs for 2pFLIM. Furthermore, tAKARα detected physiologically-relevant PKA activity elicited by multiple neuromodulators, and the expression of tAKARα did not alter neuronal functions[17].

Recently, tAKARα was successfully used to visualize PKA activities in head-fixed behaving mice[17]. It was shown that enforced locomotion triggered PKA activity in the soma of superficial layer neurons (layer 1 through 3, up to a depth of ~300 μm from pia) in the motor, barrel, and visual cortices. The locomotion-triggered PKA activity was in part dependent on signaling via β-adrenergic receptors and D1 dopamine receptors, but was not affected by a D2 dopamine receptor antagonist. This work illustrates the ability of tAKARs to track neuromodulation events in vivo using 2pFLIM.

In the current protocol, the entire method for PKA activity imaging in head-fixed awake mice during an enforced locomotion paradigm is described in six steps. First, the addition of

2pFLIM capabilities to a conventional two-photon microscope (Figure 1). Second, the construction of a motorized treadmill (Figure 2). Third, the expression of the tAKARα sensor in the mouse cortex by in utero electroporation (IUE) of DNA plasmids, or stereotaxic injection of adeno-associated virus (AAV). Excellent protocols for surgeries for IUE[24,25] and stereotaxic injection of viral particles[26] have been previously published. The key parameters we used are described below. Forth, the installation of a cranial window. Excellent protocols have been previously published for cranial window surgery[27,28]. Several steps that have been modified from the standard protocols are described. Fifth, performing in vivo 2pFLIM. Sixth, the analyses of 2pFLIM images (Figure 3 and Figure 4). This approach should be readily applicable to many other head-fixed behavioral paradigms and brain areas.

Protocol

All methods described here have been approved by the Institutional Animal Care and Use Committee (IACUC) of Oregon Health and Science University.

1. 2pFLIM Microscope Setup

1. Install a photon timing counting module (PTCM, Table of Materials) and connect to the computer (Figure 1) according to the manufacturer's manual.

   NOTE: The PTCM is typically a computer board that receives a "sync" input for the laser pulse timing and a photon input from the photomultiplier tube (PMT). It also receives clock timing for pixels, lines, and frames, from two-photon imaging control software. The PTCM uses the clock signals to separate individual photons into different pixels and frames.

2. Add a photodiode with >200 MHz bandwidth to measure the laser timing. Place a standard glass coverslip in the light path to reflect a small fraction of the laser light into the photodiode placed perpendicular to the light path (Figure 1). Connect the photodiode output to the "sync" input of the PTCM.

   NOTE: Many modern lasers also output the laser timing. For these lasers, the photodiode is not necessary, and one can directly connect the laser timing output to the sync input of the PTCM.

3. Exchange the PMT, in case of the tAKARα, the green channel PMT, with a low-noise, fast GaAsP PMT (Figure 1). Connect the PMT output to the signal input of the PTCM.

   1. Add an optional signal splitter (Figure 1) if simultaneous acquisition of intensity through the conventional two-photon imaging channel is desired. Connect the PMT output to the signal splitter and connect the splitter output to the PTCM and the conventional two-photon imaging module.

      NOTE: GaAsP PMTs give faster single-photon signals than conventional bialkali PMTs and allow for a more precise determination of the photon timing. Certain models of GaAsP PMTs can be cooled to 10–35 °C below ambient temperature, allowing the suppression of dark

counts to a level below a few hundred per second (typically ≤200 counts/s). This low noise level is important for the precise measurement of fluorescence lifetimes because noise photon counts cannot be easily distinguished or subtracted from the fluorescence lifetime curve.

4. Add a band-pass fluorescence emission filter that minimizes the spectral contamination, if any, from the acceptor fluorophore. For example, for tAKARα, a 500 nm ± 20 nm barrier filter for the green channel is used to reduce the contamination from the acceptor sREACh, which is a dark (QY ~0.07) yellow fluorescent protein (YFP)[29,30]. Connect timing signals, such as the clocks for individual image pixels, lines, and frames, as appropriate to the control software and described in the PTCM user manual. Install the appropriate data control and acquisition software.

   NOTE: Some PTCM manufacturers (Table of Materials) provide their software for 2pFLIM imaging. Here, custom software called FLIMimage is used, which was developed by the Yasuda Lab (Max Planck Florida, via personal communication). This software functions as an add-on user function to certain two-photon acquisition software (Table of Materials). It controls and communicates with the PTCM at the appropriate timing during two-photon imaging to acquire 2pFLIM images.

2. Construction of a Motorized Treadmill

NOTE: The design of the custom-built motorized treadmill is shown in Figure 2.

1. Cut a foam roller (Ø = 200 mm) to 150 mm in length with a fine hacksaw. Alternatively, glue the two halves of a foam ball together and place tape over the seam. Optionally, glue a rubber mat with profile on the roller to increase traction on the roller.

2. Drill a ¼ inch diameter hole through the center of the roller at the flat side of the roller or drill a ¼ inch diameter hole through the middle of each half of the ball if the foam ball is used.

3. Install a ¼ inch diameter steel axle through the hole. Glue the foam roller/ball to the axle using foam-compatible glue. Optionally, modify two flexible shaft couplings (¼ inch inner diameter) to strengthen the coupling of the axle to the foam roller/ball.

   NOTE: Please note that many common glues may dissolve foam.

   1. For each shaft coupling, position the shaft coupling on its flat side and at the center of the rectangle metal plate (0.7 mm × 15 mm × 76 mm). Weld the plate to the shaft coupling. Drill a ¼ inch hole at the center of the plate to allow for installation of the modified shaft coupling on to the axle and two screw holes into the metal plate lateral from the center.

2. Install the shaft coupling onto the axle against the foam roller/ball. If using the latter, slightly bend the plate to fit the curvature of the ball. Place screws into the lateral holes to fix the roller/ball on the axle.

4. Drill and tap a 3/8–32 thread at the center of a cage plate and install the rotary encoder. Drill a screw hole into the base of the right-angle motor bracket to allow attachment of the motor onto the post holder. Attach both the rotary encoder and the motor to the end of the axle using a flexible shaft coupling.

5. Install the assembled treadmill on an aluminum bread board using posts for the motor and rotary encoder (Figure 2). Connect the motor inputs to the speed controller, and the rotary encoder output to an analog input of the computer data acquisition (DAQ) board.

   NOTE: The rotation angular speed is encoded by the rotary encoder as voltage and is digitized using custom software called AnimalTracker written in MATLAB.

6. Install the headplate-compatible holder to a right-angle bracket. Install a solid post on the bread plate in front of the treadmill and install the assembled headplate holder with the right-angle bracket on the post (Figure 2). Ensure that the headplate holder bars are aligned with the axle such that the mouse can adopt an adequate and comfortable walking position on the treadmill (Figure 2C).

3. Expression of tAKARα Sensor in the Mouse Cortex

1. In utero electroporation

   1. Prepare a DNA solution for IUE by adding 0.2% final concentration of fast green dye (for visualization during injection) to a plasmid DNA (3–4 μg/μL; the sensor constructs containing a CAG promotor, sensor sequence, and a woodchuck hepatitis virus posttranscriptional response element [WPRE] translational enhancer) dissolved/diluted in water or Tris-EDTA.

   2. Prepare a timed pregnant female mouse (e.g., C57BL/6) for IUE at E16[24]. Anesthetize the mouse with isoflurane (4% for induction and 1.5% for maintenance, on 95% O2 with 5% CO_2) and apply subcutaneous injection of peri-operative analgesics containing 5 mg/ kg Meloxicam and 4 mg/kg Bupivacaine. Cut open the abdominal cavity with a scalpel and a pair of scissors and carefully expose the uterine horns.

   3. Inject 1 μL of DNA solution per embryo in the lateral ventricle of one hemisphere, as previously described[24].

   4. Perform regular IUE[24] for cortical neurons by placing the positive electrode end foot at the cortex and using five 100-ms square pulses (38 V) at 1 Hz with an electroporator.

NOTE: Different cortical regions can be targeted for electroporation by changing the placement of the electrode end foot relative to the lateral ventricle.

2. Stereotaxic injection

    1. Prepare a mouse at postnatal day 30 for stereotaxic surgery[26]. Anesthetize the mouse as described in step 3.1.2., and apply subcutaneous injection of peri-operative analgesics containing 5 mg/kg Carprofen.

    2. Dilute AAV serotype 2/1 (AAV2/1) expressing hSyn-tAKARα-WPRE to an empirically determined titer (~1×10^9–1×10^{10} genomes/μL) in syringe-filtered (0.2 μm cellulose acetate membrane) phosphate-buffered saline.

    3. Drill a ~500 μm diameter hole using a handheld drill under a stereomicroscope at the following coordinates for the motor cortex: 0.5 mm anterior to bregma, 1.2 mm lateral to midline.

    4. Mount an injector (e.g., oil hydraulic manipulator, with custom-made plunger/glass pipette holder) to a motorized manipulator. Place the injection needle at a 15° angle relative to the bregma-lambda plane. Program a diagonal movement across the x- and z- axes equivalent to a 700 μm and 200 μm progression along the anterior-posterior and dorsal-ventral axes, respectively.

        NOTE: To avoid damage to the tissue directly above the intended imaging field, AAV particles are injected at an angle relative to the bregma-lambda plane.

    5. Position the tip of the injection needle at the pia in the center of the drill hole and slowly execute the diagonal movement (~25 μm/s) described above. This procedure will position the center of injection at 1.2 mm anterior to bregma, 1.2 mm lateral to midline, 0.2 mm below the pia.

    6. Inject 20 nL of diluted viral particles (~10 nL/min). Wait at least 10 min and slowly retract the injection needle (~12.5 μm/s).

    7. Finish the stereotaxic injection procedure and glue/suture the skin[26].

4. Installation of the Cranial Window

1. Perform the placement of the cranial window on mice expressing tAKARα via IUE (section 3.1) or stereotaxic injection of viral particles (section 3.2), between postnatal days 30 and 60. For mouse infected with viral particles, implement the cranial window at least two weeks after the virus injection. Install the cranial window as previously described[27,28], with the following details. Anesthetize the mouse as described in step 3.1.2., and apply subcutaneous injection of peri-operative analgesics 0.075 mg/kg Buprenex and anti-inflammatory agent Dexamethasone at 4 mg/kg.

2. Remove the periosteum and retract the neck muscle. Glue the edge of the skin to the skull with tissue adhesive to avoid exposure of the neck musculature after surgery.

3. Dry and remove any periosteum from the skull by gently scraping using a scalpel. Place the imaging headplate (8 mm inner diameter) to surround the intended imaging field. Glue the headplate to the skull using cyanoacrylate-based glue, followed by dental acrylic cement. For optimal adhesion, ensure that the headplate rests on the exposed and dried skull. Glue accelerator can be used to accelerate the hardening.

4. Draw a circle of 5 mm in diameter above the intended imaging field (coordinates as specified in step 3.2.3) using a dental drill and expose the dura mater.

5. Apply a thin layer of transparent polymer, also called artificial dura, to the dura surface to cover the entire cranial window. The polymer will protect and stabilize the dura mater. Place a sterile circular coverslip (5 mm diameter) on the dura mater. Secure the coverslip with cyanoacrylate glue applied around the edges of the window followed by dental acrylic cement.

5. In Vivo Two-photon Fluorescence Lifetime Imaging Microscopy

1. Commence 2pFLIM imaging at or beyond 2 weeks post-installation of the cranial window (section 4). Minimize experimental interference due to stress by frequent handling and scruffing of the mouse prior to the start of the imaging study to habituate the mouse.

2. Set the two-photon excitation laser wavelength to 960 nm using the software that controls the two-photon laser.

3. Anaesthetize the mouse using 4% isoflurane. Confirm proper anesthetization by tail-pinch and observing breathing rates. That is, there should be no response to the tail-pinch and the breathing rate should be reduced to ~1 breath per second. To minimize unnecessary procedural time and because the anesthesia lasts only for two to three minutes, eye lubricants are not used.

4. Transfer the anaesthetized mouse to the motorized treadmill (Figure 2C) and mount the headplate of the mouse to the headplate holder of the treadmill setup (see Figure 2 for details). Clean the surface of the cranial window coverslip on the mouse with 70% ethanol.

5. Place the motorized treadmill with the mounted mouse under the 2pFLIM objective. Apply a drop of distilled water between the cranial window coverslip and the objective.

6. Let the mounted mouse wake up from anesthesia and become acclimated to the treadmill and microscope environment for at least 10 min. Monitor respiration rate of the mouse while the mounted mouse wakes up from anesthesia.

7. Navigate to the injection location under epi-illumination. Document fiducial features (i.e., blood vessels) under brightfield to aid imaging of the same region of interest (ROI) during subsequent imaging sessions.

8. Eliminate any incoming light other than the emitted light from the brain tissue. Switch off the epi-illumination light source and close the enclosure of the 2pFLIM rig. Activate the 2pFLIM PMT by switching on the hardware command voltage control.

9. Acquire a z-stack 2pFLIM image using the 2pFLIM acquisition software FLIMimage with the following recommended settings for imaging tAKARα-positive somata in awake mice. Set frame averaging to 3 frames, scanning speed to 2 ms/line, image size to 128 × 128 pixels, and field of view to 90–100 μm. Adjust imaging settings based on the preparation and hardware configuration.

10. Inspect the acquired image in FLIMview (in-house developed custom software; see section 6). Adjust imaging settings following step 5.9 to optimize photon count and minimize photobleaching.

    NOTE: A workable integrated photon count in an ROI for lifetime imaging of a tAKARα-positive soma in vivo is ~1,000–10,000 photons depending on the signal amplitude that results from a particular stimulus (see Discussion).

    1. Where needed, use a decreased field of view, decreased scanning speed, increased laser power, and increased number of frames to be averaged to increase the integrated photon counts and reduce the lifetime estimation error. At the same time, be sure to use the minimal essential laser power, frame averaging, and scanning speed to minimize photobleaching.

11. Image at a regular time interval (e.g., every 30–60 s) by repeating the z-stack acquisition using settings determined in step 5.10. Acquire baseline 2pFLIM images for at least 15 min at zero treadmill speed.

12. Set the treadmill rotation speed to ~15 cm/s for 15 min while acquiring 2pFLIM images. Continue imaging for ≥20 min after switching off the treadmill rotation, to assess the duration of PKA activity after cessation of forced locomotion.

6. Analysis of 2pFLIM Images

1. Open the acquired images in FLIMview and set the following parameters in the FLIMview.

   NOTE: Parameter details are described in DISCUSSION.

   1. Click on the single photon counting (SPC) minimum and maximum range fields in FLIMview. Enter the appropriate minimum and maximum SPC range value, typically ranging between 1.2–2 and 10–12 ns, respectively.

2. Click on the t_0 value field in FLIMview and enter the t_0 value (typically ~2 ns). Click on the lifetime luminance minimum threshold value field in FLIMview and enter the desired threshold value to 5–30 photons.

2. Click on the new group button (**N**) and assign an experiment group name. This will generate a group that combines data from each added FLIM image.

3. Click on the **ROI** button in the **Roi Controls** module of FLIMview and draw an ROI around a tAKARα-positive soma. Reduce the z-stack range, by moving the lower and upper z-limit in the **z-stack Control** sliders in FLIMview, to minimize signal contamination originating from background photons in other z depths.

4. Click on the **+** button to add the FLIM image to the group (step 6.2). Click on the **Calc** button to calculate the mean lifetime (LT, also called mean photon emission time [MPET]), for the ROI and the lifetime estimation error ($\delta\tau$).

5. Open the next file in the chronical 2pFLIM imaging series. Repeat step 6.4. Be sure to adjust the position of the ROI and z-stack range to measure the same tAKARα-positive soma over time, because there can be tissue drift over time.

6. Select the **deltaMPET/MPET$_0$** in the drop-down menu of the **Group Controls** module. Click on the **baseline#** field and enter the index(es) (e.g., **1 2 3 4 5** for the first five images in the group created in step 6.3). This will define the image(s) used to calculate baseline lifetime (LT_0).

7. Click on **Plot** to generate a graph containing the FLIM response ($\Delta LT/LT_0$) of tAKARα during the experiment in the defined ROIs. Normalized changes in lifetime (ΔLT) of individual ROIs by the corresponding baseline lifetime (LT_0) allow for comparison of PKA activity during locomotion across different ROIs.

Representative Results

FRET-FLIM sensors allow for the visualization of many different signaling pathways, including the cAMP/PKA pathway involved in neuromodulation. The current protocol utilizes the recently-developed tAKARα sensor in combination with 2pFLIM to visualize PKA activities in head-fixed behaving mice. Most existing two-photon microscopes can be upgraded with 2pFLIM capabilities by adding three to four components, as illustrated in Figure 1 (see also section 1). To visualize FRET in 2pFLIM-acquired images, quantification of mean lifetime was performed on histogram plots of photon timing collected per pixel (Figure 3A,B). Mean lifetime was visualized using a pseudo-colored image, in which high (cold color) and low (warm color) mean lifetimes represent low and high PKA activities, respectively, since PKA activation leads to the decrease of lifetime. Care must be taken to set the SPC range correctly; this range should be set within the laser pulse interval (e.g., 12.5 ns of a pulse rate of 80 MHz) with minimized hardware edge artifacts (see also section 6 and DISCUSSION). Calculation of PKA activity within ROIs was performed by combining the LT of all pixels within a given ROI (Figure 3C,D). In head-fixed awake mice basal lifetimes ranged between 1.3 and 1.8 ns (Figure 3E). Imaging of tAKARα in the motor cortex in head-fixed awake mice allowed for the real-time quantification of PKA activity with cellular resolution during basal and enforced locomotion (Figure 4). The experiment can be repeated

over days and months. Enforced locomotion triggers PKA activity in a population of neurons within the superficial layers of the mouse motor cortex[17]. This PKA activity is dependent on neuromodulation via activation of β-adrenergic and D1 receptors[17].

Discussion

This protocol demonstrates the use of FRET-FLIM sensor tAKARα to visualize neuromodulation-triggered PKA activity in head-fixed behaving mice. This application is based on extensive testing and characterizations of tAKARα in vitro and in vivo to demonstrate that the FLIM signal obtained is relevant to physiological neuromodulatory events[17]. Here, one in vivo application, locomotion-induced PKA activity in the motor cortex, is used to describe the procedures for delivering the sensor to the brain, animal surgery for imaging, hardware and software requirements for behavior and imaging data acquisition, and software and algorithms for imaging data analyses.

The tAKARα sensor is introduced to the cortex by IUE of DNA plasmids or stereotaxic injection of AAV particles. Depending on the electroporation parameters and DNA concentrations, IUE results in various labeling density of cortical neurons over a relatively large area in the cortex[25]. The cortical layer labeled using IUE is determined by the embryonic stage when the surgery is performed. Stereotaxic injection of AAV particles is used when it is desired to image many cells within a defined brain subregion. It typically results in densely labeled neurons at the injection center and increasingly sparse labeling further from the center. Importantly, infection efficiency of cells within the brain is dependent on the AAV serotype used. AAV2/1 offers great efficiency in cortical, thalamic, and striatal neurons with relatively low retrograde labeling activities. It is advised to empirically establish which AAV serotype is most efficient for the targeted brain region and cell type. Both transfection methods have successfully expressed tAKARα. The “sweet spot” for the expression level is empirically determined.

Enforced locomotion results in increased PKA activities in layer 2/3 neurons of the motor cortex. Currently, 2pFLIM limits the range of testable behaviors due to head-fixation of the mouse. However, an ever-growing list of behavioral paradigms have been successfully implemented within this constraint, ranging from reporting stimuli in go/no-go tasks to spatial orientation in virtual reality[31,32,33]. In addition, improved methods may enable imaging in deep brain regions, such as the striatum, amygdala, and hippocampus, via a needle-like gradient index (GRIN) lens[13] (unpublished observations). Therefore, the present protocol detailing the use of tAKARα and 2pFLIM for in vivo visualization of neuromodulation events should be readily applicable to many brain regions in the context of head-fixed behavioral paradigms.

Calculation of lifetime per pixel or ROI using curve fitting is computationally time consuming, and the limited total photon count per pixel often results in fitting errors. Hence, mean lifetime (LT) is arithmetically calculated as an approximation for the lifetime (τ)[17,34]:

$$\mathrm{LT} = \frac{\int_{SPC_{min}}^{SPC_{max}} tF(t)dt}{\int_{SPC_{min}}^{SPC_{max}} F(t)dt} - t_0 \quad \text{(Equation 1)}$$

where SPC_{min}, and SPC_{max} are the measurement window (SPC) borders and F(t) is the fluorescence lifetime decay curve. In other words, for each calculated volume (pixel or ROI, Figure 3A) the photon timing distribution is plotted in a histogram (Figure 3B). Within the SPC range the weighted integral (with time being the weight) of this distribution is divided by the total photon count to result in an averaged emission time. This time is then corrected for t_0. To generate a lifetime image (Figure 3A) this procedure is performed for each pixel, whereas calculation of lifetime per ROI (Figure 3C,D) integrates all photons from all pixels that are above threshold within the ROI volume. The lifetime estimation error ($\delta\tau$) is calculated using the integrated intensity (N_{photon}: total photon count):

$$\delta\tau \approx \frac{\tau}{\sqrt{N_{photon}}} \quad \text{(Equation 2)}$$

To minimize lifetime estimation error, $\delta\tau$, and yield proper signal detection FRET-FLIM requires the acquisition of enough photons per ROI. In order to achieve a desired signal-to-noise ratio (SNR), $\delta\tau$ also have to meet the following equation:

$$\delta\tau \leq \frac{\Delta LT}{SNR} \quad \text{(Equation 3)}$$

For example, typical measurement during locomotion in a neuronal soma in the motor cortex (LT = 1.57 ns, N_{photon} = 9075, ΔLT = 0.15 ns; Figure 4, cell 1) yields a lifetime estimation error of:

$$\delta\tau \approx \frac{1.57}{\sqrt{9075}} \approx 0.016 \text{ ns} \quad \text{(Equation 4)}$$

which results in a signal-to-noise ratio of:

$$\mathrm{SNR} \approx \frac{\Delta LT}{\delta\tau} = \frac{0.15}{0.016} \approx 9.4 \quad \text{(Equation 5)}$$

If a desired SNR is only 5, given ΔLT = 0.15 ns a $\delta\tau$ is allowed of:

$$\delta\tau \approx \frac{\Delta LT}{SNR} = \frac{0.15}{5} \approx 0.03 \text{ ns} \quad \text{(Equation 6)}$$

which requires a minimum total photon count of:

$$N_{photon} \approx \left(\frac{LT}{\delta\tau}\right)^2 = \left(\frac{1.57}{0.03}\right)^2 \approx 2739 \text{ photons} \quad \text{(Equation 7)}$$

As outlined above, lifetime quantification requires appropriately setting several parameters, such as SPC range, t_0, and lifetime luminance minimum threshold. The SPC range determines the measurement window of emitted photons within the hardware measurement window (Equation 1; hardware measurement window is typically 0–12.5 ns, as the laser repeats at 80 MHz). This is necessary because the PTCM used in this protocol has edge artifacts. The SPC range is set to incorporate most of the donor photon lifetime distribution without including the edge artifacts. To calculate mean lifetime, the mean photon timing from the measurement window is subtracted by t_0, which corresponds to the timing of the laser pulse within the window (Equation 1, Figure 3A,B)[17,34]. t_0 can be adjusted by changing the signal cable lengths or the PTCM settings, and is typically adjusted to be ~2 ns from the start of the hardware measurement window. After initial characterization of the system, typically carried out under near ideal imaging conditions (e.g., when imaging 5 μM fluorescein solution), both the SPC range and t_0 are set as fixed parameters of a given hardware configuration. Lifetime luminance minimum threshold is set so that only pixels with a total photon count equal or higher than the threshold will be included in display and analysis. This effectively reduces the noise due to background photon counts, including autofluorescence, ambient light, and spontaneous PMT dark counts. This threshold is empirically determined.

Successful FRET-FLIM sensors for in vivo 2pFLIM imaging have at least three common features. First, regarding the selection of fluorophores, the photon collection efficiency is usually low under the challenging in vivo imaging environment in part due to severe light scattering in brain tissue. At the same time, a high number of detected photons is required to achieve a desirable SNR (≥1,000 photons would be required to achieve a SNR of 1 for a $\Delta LT/LT_0$ of 0.03; see Equations 2 and 3). Therefore, a donor fluorophore with a high photon budget (i.e., the maximal number of detectable photons before a fluorophore is bleached) is favored. Currently, there is no systematic comparison of different donor fluorophores in terms of their photon budget under two-photon excitation. Empirically, eGFP is relatively bright while being more photostable compared to many other fluorophores in the green/yellow spectrum, making it a great donor fluorophore for in vivo use of FRET-FLIM sensors. In addition, for optimal quantification of FRET, donor fluorophores with a single-exponential fluorescence lifetime decay are favored. Many commonly-used donor fluorescent proteins for ratiometric imaging, such as eCFP, have multi-exponential fluorescence lifetime decays, suggesting that they consist of mixed populations of fluorophores. These fluorescent proteins are therefore not ideal for FRET-FLIM[21]. Contrary to the donor fluorophore, a low quantum yield of the acceptor fluorophore can be beneficial for FRET-FLIM sensors. The “dark” low-irradiant fluorophore sREACh is used for tAKARs. Low quantum yield of the acceptor fluorophore minimizes photon contamination in the donor fluorophore emission spectrum and frees one fluorescence detection channel for simultaneous imaging of a second fluorescent sensor or morphology marker in the red spectrum in the case of tAKARα.

Second, to obtain sufficient SNR across the binding fraction range, an optimal FRET-efficiency of ~0.5–0.7 is favored[21]. The signal, i.e., the mean lifetime change under a given donor-acceptor binding ratio change, is dependent on the efficiency of FRET. This relationship between FRET efficiency and mean lifetime change is, however, non-linear. If

the FRET efficiency approaches one, the donor fluorophores in bound-state are effectively emitting nearly no photons. Therefore, unless the binding ratio is 100% (this is never the case because no acceptor fluorophore matures to 100%[29]) the mean lifetime approaches the lifetime of the donor fluorophore in open-state, and the ability of detecting bound-state sensors decreases. The FRET-efficiency for tAKARα is estimated to be ~0.7, within the favorable range.

Third, FRET-FLIM sensors should report signals with a sensitivity and kinetics that are relevant to animal physiology. Sensor sensitivity and kinetics should be extensively tested in vitro prior to its use in vivo, and, if necessary, can be tuned using a variety of approaches, such as adjusting substrate-binding domain affinity and kinetics, linker-optimization, and subcellular targeting of the sensor. In previous work, it was established that tAKARα can detect PKA activity elicited by the releases of endogenous dopamine, and that the kinetics and sensitivity of the sensor align with a known PKA-dependent biological process, which is norepinephrine-induced inactivation of the slow after-hyperpolarization current[17]. Furthermore, the expression of tAKARα does not appear to alter neuronal functions, as assayed by electrophysiology[17] and measurement of structural plasticity of individual spines (unpublished observations).

Current technical limitations of 2pFLIM imaging are related to data handling and photon counting throughputs. First, FLIM requires the storage of photon arrival times for each pixel. The memory size of the PTCM limits the obtainable pixel resolution. For the PCTM described here, up to 256 × 256 pixels per image frame with a 64-point time resolution can be achieved. In addition, the transfer speed of FLIM image data from board to computer storage is relatively slow, again, putting practical limits on the resolution and sampling frequency. Continuous technological improvement of memory capacity and data handling may resolve these limitations in the future. Second, commonly-used PTCMs are analog-to-digital systems and are limited by their photon detection reset times (i.e., “dead time”). This means that after the detection of one photon the PTCM will not register the arrival of any subsequent photon(s) for the next 100–125 ns[18,21]. Furthermore, the lifetime measurement is biased towards the first arrived photon after a laser pulse (so called “pile-up”). These limit the photon counting rates to $<10^7$ photons per s. Although in most typical two-photon imaging regimes this is not a major problem, care should be taken not to exceed the photon counting rate limits. Newer PTCMs that have shorter dead time or a gigahertz continuous data acquisition system can alleviate this limitation (for the latter see Yellen and Mongeon[18]).

Fluorescent sensors for signaling pathways, such as cAMP/PKA, Akt/PKB, PKC, and ERK, are continuously being generated and optimized[16,35]. For most of the current sensors, further characterization and optimization are needed to excel in the challenging in vivo imaging environment. In particular, increased signal amplitude is important, as any increase in the signal amplitude reduces the demand on photon budgets with a square relationship. For tAKARα, its response amplitude to endogenous neuromodulators, such as norepinephrine, was improved by 2.7-fold compared to the previous best sensor. This translated to a ~7-fold decrease in required photons. In practice, this greatly reduced the number of false negatives (i.e., non-responders) in animals during behavior[17]. The maximum tAKARα signal

observed is ~30% ($\Delta LT/LT_0$). To date, this is the largest FLIM signal reported for similar classes of FRET sensors. Further improvement may also be possible by optimizing the acceptor fluorophore and the affinity of the FHA to the phosphorylated threonine. In addition, the use of sensors that monitor different aspects of the same signaling pathway may provide a powerful approach to mechanistically investigate the regulation of the signaling pathways in vivo. In the future, the successful application of FLIM sensors to visualize neuromodulatory signaling pathways in vivo will provide important insights regarding where and when neuromodulation takes place in intact neuronal networks of behaving mice.

Supplementary Material

Refer to Web version on PubMed Central for supplementary material.

Acknowledgments

We thank Ms. Tess J. Lameyer, Ms. Ruth Frank, and Dr. Michael A. Muniak for edits and comments, and Dr.Ryohei Yasuda at Max Planck Florida for 2pFLIM acquisition software. This work was supported by two BRAIN Initiative awards U01NS094247 (H.Z. and T.M.) and R01NS104944 (H.Z. and T.M.), an R01 grant R01NS081071 (T.M.), and an R21 grant R21NS097856 (H.Z.). All awards are from the National Institute of Neurological Disorders and Stroke, United States.

References

1. Greengard P The Neurobiology of Slow Synaptic Transmission. Science.294 (5544), 1024–1030 (2001). [PubMed: 11691979]
2. Petersen SE, Posner MI The attention system of the human brain: 20 years after. Annual Review of Neuroscience.35 (2), 73–89 (2012).
3. Sun Y, Hunt S, Sah P Norepinephrine and Corticotropin-Releasing Hormone: Partners in the Neural Circuits that Underpin Stress and Anxiety. Neuron.87 (3), 468–470 (2015). [PubMed: 26247856]
4. Berke JD What does dopamine mean? Nature Neuroscience.21 (6), 787–793 (2018). [PubMed: 29760524]
5. Chen Y et al. Endogenous Gαq-Coupled Neuromodulator Receptors Activate Protein Kinase A. Neuron.96 (5), 1070–1083 (2017). [PubMed: 29154125]
6. Madison DV, Nicoll RA Cyclic adenosine 3',5'-monophosphate mediates beta-receptor actions of noradrenaline in rat hippocampal pyramidal cells. The Journal of Physiology.372 (1), 245–259 (1986). [PubMed: 2425084]
7. Yasuda H, Barth AL, Stellwagen D, Malenka RC A developmental switch in the signaling cascades for LTP induction. Nature Neuroscience.6 (1), 15–16 (2003). [PubMed: 12469130]
8. Pedarzani P, Storm JF PKA mediates the effects of monoamine transmitters on the K+ current underlying the slow spike frequency adaptation in hippocampal neurons. Neuron.11 (6), 1023–35 (1993). [PubMed: 8274274]
9. Brandon EP, Idzerda RL, McKnight GS PKA isoforms, neural pathways, and behaviour: making the connection. Current Opinion in Neurobiology.7 (3), 397–403 (1997). [PubMed: 9232801]
10. Radnikow G, Feldmeyer D Layer- and Cell Type-Specific Modulation of Excitatory Neuronal Activity in the Neocortex. Frontiers in Neuroanatomy.12 (1), (2018).
11. Kennedy RT Emerging trends in in vivo neurochemical monitoring by microdialysis. Current Opinion in Chemical Biology.17 (5), 860–867 (2013). [PubMed: 23856056]
12. Rodeberg NT, Sandberg SG, Johnson JA, Phillips PEM, Wightman RM Hitchhiker's Guide to Voltammetry: Acute and Chronic Electrodes for In Vivo Fast-Scan Cyclic Voltammetry. ACS Chemical Neuroscience.8, (2), 221–234 (2017). [PubMed: 28127962]

13. Hamel EJO, Grewe BF, Parker JG, Schnitzer MJ Cellular level brain imaging in behaving mammals: An engineering approach. Neuron.86 (1), 140–159 (2015). [PubMed: 25856491]
14. Allen MD, Zhang J Subcellular dynamics of protein kinase A activity visualized by FRET-based reporters. Biochemical and Biophysical Research Communications.348 (2), 716–721 (2006). [PubMed: 16895723]
15. Zhang J, Ma Y, Taylor SS, Tsien RY Genetically encoded reporters of protein kinase A activity reveal impact of substrate tethering. Proceedings of the National Academy of Sciences of the United States of America.98 (26), 14997–5002 (2001). [PubMed: 11752448]
16. Chen Y, Saulnier JL, Yellen G, Sabatini BL A PKA activity sensor for quantitative analysis of endogenous GPCR signaling via 2-photon FRET-FLIM imaging. Frontiers in Pharmacology.5 (4), 1–12 (2014). [PubMed: 24478702]
17. Ma L et al. A Highly Sensitive A-Kinase Activity Reporter for Imaging Neuromodulatory Events in Awake Mice. Neuron.99 (4), 665–679 (2018). [PubMed: 30100256]
18. Yellen G, Mongeon R Quantitative two-photon imaging of fluorescent biosensors. Current Opinion in Chemical Biology.27, 24–30 (2015). [PubMed: 26079046]
19. Tang S, Yasuda R Imaging ERK and PKA Activation in Single Dendritic Spines during Structural Plasticity. Neuron.93, (6) 1315–1324 (2017). [PubMed: 28285819]
20. Tillo SE et al. Liberated PKA Catalytic Subunits Associate with the Membrane via Myristoylation to Preferentially Phosphorylate Membrane Substrates. Cell Reports.19 (3), 617–629 (2017). [PubMed: 28423323]
21. Yasuda R Imaging spatiotemporal dynamics of neuronal signaling using fluorescence resonance energy transfer and fluorescence lifetime imaging microscopy. Current Opinion in Neurobiology.16 (5), 551–561 (2006). [PubMed: 16971112]
22. Theurkauf WE, Vallee RB Molecular characterization of the cAMP-dependent protein kinase bound to microtubule-associated protein 2. Journal of Biological Chemistry.257 (6), 3284–3290 (1982). [PubMed: 6277931]
23. Zhong H et al. Subcellular dynamics of type II PKA in neurons. Neuron.62 (3), 363–374 (2009). [PubMed: 19447092]
24. Borrell V, Yoshimura Y, Callaway EM Targeted gene delivery to telencephalic inhibitory neurons by directional in utero electroporation. Journal of Neuroscience Methods. 143 (2), 151–158 (2005). [PubMed: 15814147]
25. Baumgart J, Baumgart N Cortex-, Hippocampus-, Thalamus-, Hypothalamus-, Lateral Septal Nucleus- and Striatum-specific In utero Electroporation in the C57BL/6 Mouse. Journal of Visualized Experiments. (107), e53303 (2016). [PubMed: 26862715]
26. Lowery RL, Majewska AK Intracranial Injection of Adeno-associated Viral Vectors. Journal of Visualized Experiments. (45), 1–4 (2010). [PubMed: 20164822]
27. Mostany R, Portera-Cailliau C A Craniotomy Surgery Procedure for Chronic Brain Imaging. Journal of Visualized Experiments. (12), 18–19 (2008).
28. Holtmaat A et al. Long-term, high-resolution imaging in the mouse neocortex through a chronic cranial window. Nature Protocols.4 (8), 1128–1144 (2009). [PubMed: 19617885]
29. Murakoshi H, Lee SJ, Yasuda R Highly sensitive and quantitative FRET-FLIM imaging in single dendritic spines using improved nonradiative YFP. Brain Cell Biology.36 (1–4), 31–42 (2008). [PubMed: 18512154]
30. Murakoshi H, Shibata ACE, Nakahata Y, Nabekura J A dark green fluorescent protein as an acceptor for measurement of Förster resonance energy transfer. Scientific Reports.5, 1–11 (2015).
31. Guo ZV et al. Procedures for behavioral experiments in head-fixed mice. PLoS ONE.9 (2), (2014).
32. Yu K et al. The central amygdala controls learning in the lateral amygdala. Nature Neuroscience.20 (12), 1680–1685 (2017). [PubMed: 29184202]
33. Harvey CD, Collman F, Dombeck DA, Tank DW Intracellular dynamics of hippocampal place cells during virtual navigation. Nature. 461 (7266), 941–946 (2009). [PubMed: 19829374]
34. Yasuda R Imaging intracellular signaling using two-photon fluorescent lifetime imaging microscopy. Cold Spring Harbor Protocols.7 (11), 1121–1128 (2012).

35. Mehta S et al. Single-fluorophore biosensors for sensitive and multiplexed detection of signalling activities. Nature Cell Biology.20 (10), 1215–1225 (2018). [PubMed: 30250062]

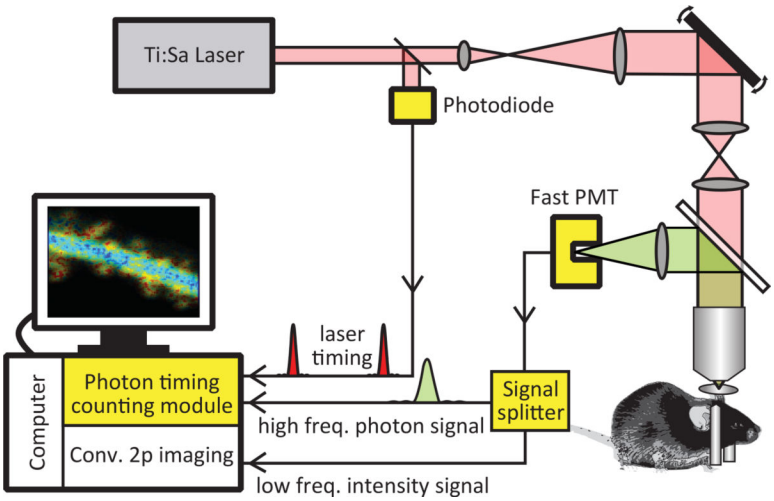

Figure 1: Schematic of a 2pFLIM system.

2pFLIM can be implemented on a conventional two-photon microscope by the addition of the yellow highlighted hardware components: a photon timing counting module, a low-noise fast photomultiplier tube (PMT), a photodiode (only needed if the laser does not have an output signaling for laser timing), and an optional signal splitter. This figure has been modified from Ma et al.[17].

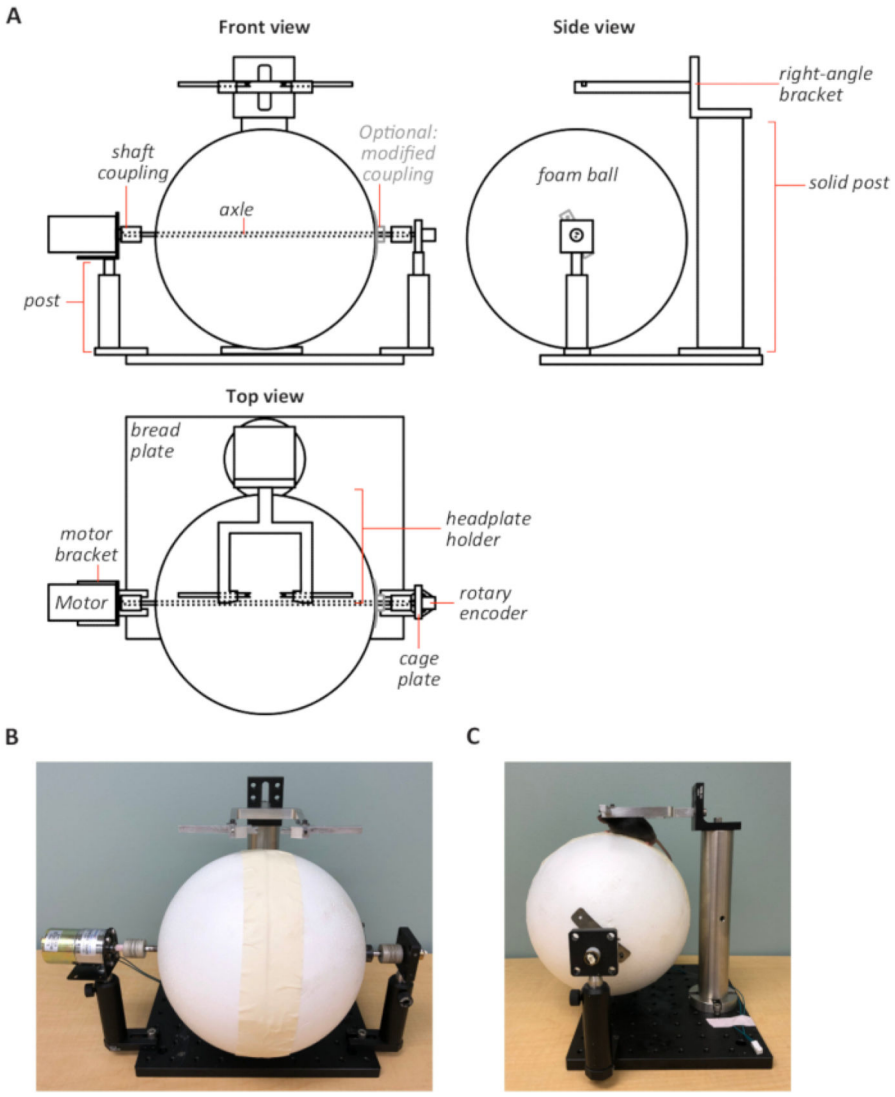

Figure 2: Design of a custom-built motorized treadmill.

(**A**) Schematic of the treadmill design from front (top left), side (top right), and top views (bottom left). The treadmill (foam ball) axle is connected to a rotary encoder and a motor that are collectively mounted on two posts on a solid aluminum bread plate. The headplate-compatible holder on right-angle bracket is fixed to a solid post and positioned above the treadmill. Schematic drawings are not to scale. Front (**B**) and side (**C**) view photographs of the treadmill. Proper positioning of the mouse on the treadmill is shown in panel **C**.

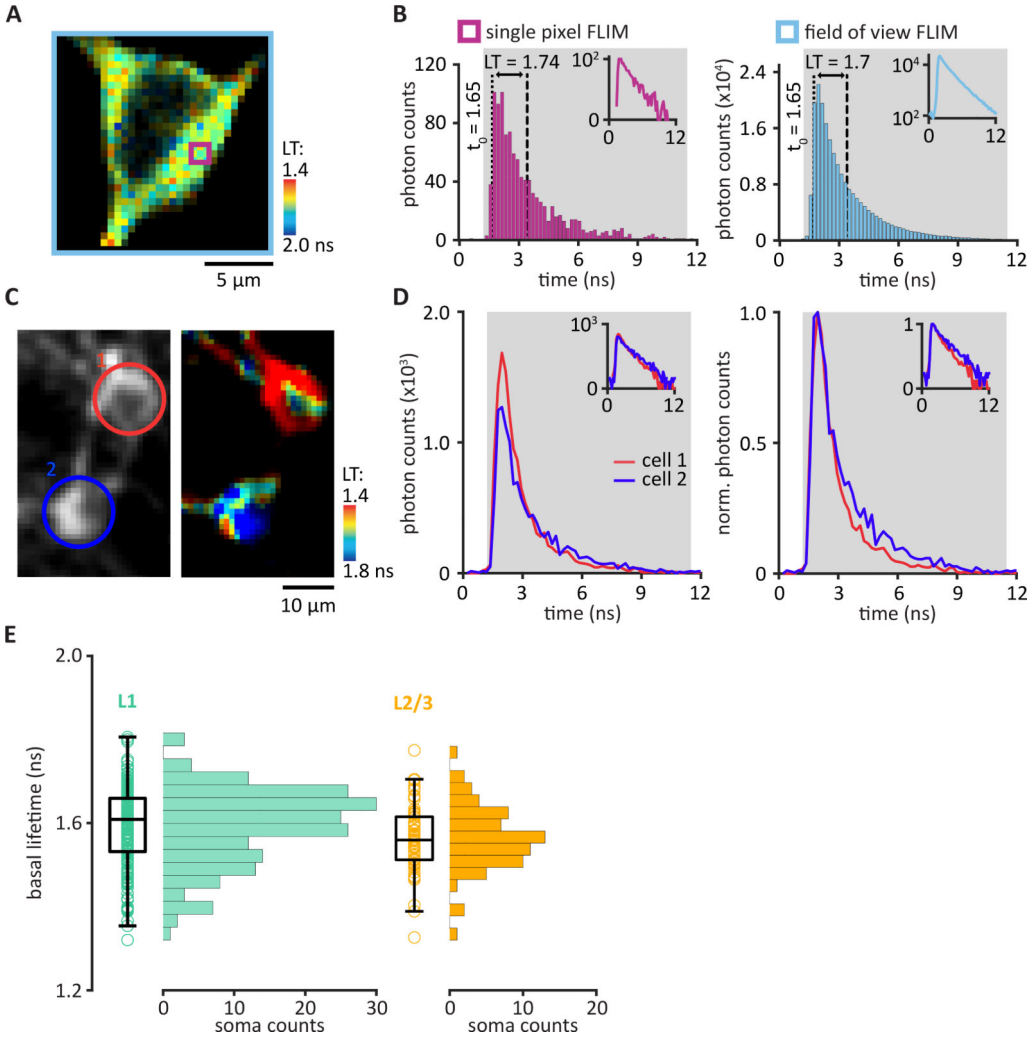

Figure 3: The quantification of 2pFLIM data.

(**A**) A FLIM image with each pixel pseudo-colored to represent the mean lifetime (LT), relative to the laser timing, of all photons in that pixel. (**B**) The photon arrival times within a single pixel (purple square in panel **A**) were plotted in a histogram (left panel). Integration boundaries were set to determine the single photon counting range (SPC, gray). Within the SPC range, the integral of photon timing was divided by the total number of photons and then subtracted by the t_0 (1.65 ns, dashed line), resulting in a mean lifetime (LT, distance between dashed and dotted lines) of 1.74 ns. Quantification of the mean lifetime of the entire field of view (light blue square in panel **A**) involved the integration of photon timing collected in all pixels (right panel), resulting in a mean lifetime of 1.7 ns. Insets show the same data in semi-log scale. (**C** and **D**) Quantification of mean lifetime per region of interest (ROI). (**C**) Representative example of a 2pFLIM image. Two ROIs were drawn around two somata in layer 2/3 of the motor cortex. (**D**) Photon timing distributions integrated across all pixels within each ROI (left panel). Cell ROIs were color-coded (as shown in panel **C**) red, cell 1; blue, cell 2. Normalized photon counts allow for comparison of photon timing distributions between the two ROIs (right panel, mean lifetime; cell 1, 1.33 ns; cell 2, 1.73 ns). Insets show the same data in semi-log scale. (**E**) Distribution plot of mean basal

lifetimes from 254 imaged cells in the superficial layers of the motor cortex. L1 cells (n = 186 cells/11 animals, left panel), residing within 100 μm below pia, expressed tAKARα after a stereotaxic injection of AAV2/1-hSyn-tAKARα-WPRE, and L2/3 pyramidal cells (n = 68 cells/4 animals, right panel), residing at least 150 μm below pia, expressed tAKARα after IUE of a CAG-tAKARα-WPRE DNA construct.

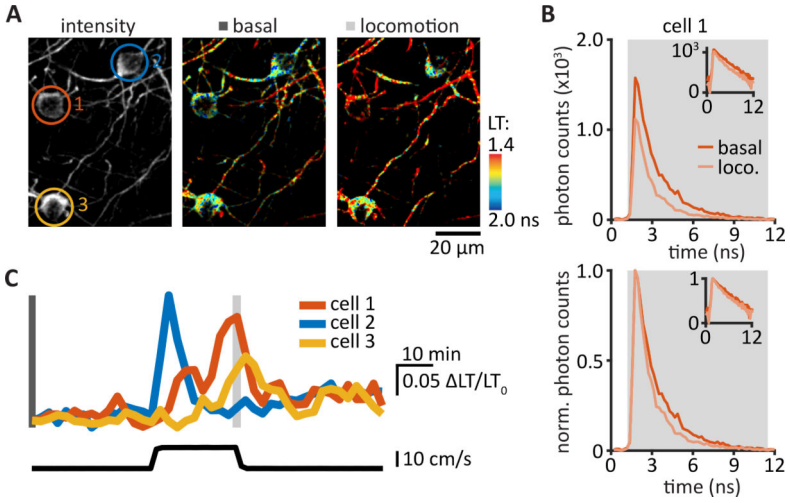

Figure 4: tAKARα tracks enforced locomotion-induced PKA activities in the motor cortex.

(**A**) Representative intensity (left panel) and lifetime (middle and right panels) images of three L1 cells in the motor cortex. Cell ROIs were color-coded: orange, cell 1; blue, cell 2; yellow, cell 3. (**B**) Photon timing distributions measured in cell 1 (upper panel) during the basal condition (orange trace, as measured in middle panel **A**) and enforced locomotion (loco., light orange trace, as measured in right panel **A**). Normalized photon counts allowed for direct comparison of photon timing distribution (lower panel, mean lifetime: basal, 1.72 ns; locomotion, 1.42 ns). Insets show the same data in semi-log scale. (**C**) Δlifetime/lifetime$_0$ ($\Delta LT/LT_0$) traces of the corresponding cells (upper panel, see panel **A**) with enforced locomotion speed (lower panel).